Journal of Structural Biology 197 (2017) 26–36

Contents lists available at ScienceDirect

Journal of Structural Biology

journal homepage: www.elsevier.com/locate/yjsbi

Probing the mechanical properties, conformational changes, and interactions of nucleic acids with magnetic tweezers

Franziska Kriegel, Niklas Ermann [1], Jan Lipfert *

Department of Physics, Nanosystems Initiative Munich, and Center for Nanoscience, LMU Munich, Amalienstr. 54, 80799 Munich, Germany

ARTICLE INFO

Article history:
Received 12 February 2016
Received in revised form 6 May 2016
Accepted 28 June 2016
Available online 29 June 2016

Keywords:
Magnetic tweezers
DNA
RNA
Persistence length
Torsional stiffness
Conformational transitions

ABSTRACT

Nucleic acids are central to the storage and transmission of genetic information. Mechanical properties, along with their sequence, both enable and fundamentally constrain the biological functions of DNA and RNA. For small deformations from the equilibrium conformations, nucleic acids are well described by an isotropic elastic rod model. However, external forces and torsional strains can induce conformational changes, giving rise to a complex force-torque phase diagram. This review focuses on magnetic tweezers as a powerful tool to precisely determine both the elastic parameters and conformational transitions of nucleic acids under external forces and torques at the single-molecule level. We review several variations of magnetic tweezers, in particular conventional magnetic tweezers, freely orbiting magnetic tweezers and magnetic torque tweezers, and discuss their characteristic capabilities. We then describe the elastic rod model for DNA and RNA and discuss conformational changes induced by mechanical stress. The focus lies on the responses to torque and twist, which are crucial in the mechanics and interactions of nucleic acids and can directly be measured using magnetic tweezers. We conclude by highlighting several recent studies of nucleic acid-protein and nucleic acid-small-molecule interactions as further applications of magnetic tweezers and give an outlook of some exciting developments to come.

1. Introduction

DNA is the carrier of genetic information in all cellular life. While much emphasis has been placed on deciphering the sequence of DNA bases, it is becoming increasingly clear that the physical properties of DNA as a polymer and polyelectrolyte play critical roles in the regulation of genetic information. In eukaryotic cells, ~2 m of DNA are packed into a ~10 μm-sized nucleus, which is achieved through numerous interactions with proteins, in particular through the hierarchical assembly of nucleosomes and higher order chromatin structures. At the same time, DNA needs to remain accessible for replication and transcription of the stored information. In addition, during linear processing of DNA, e.g. in replication, transcription, and repair, its double helical nature (Watson and Crick, 1953) naturally leads to rotational motion and the accumulation of torque. Accumulation of torque and the ensuing supercoiling of DNA are important factors in gene regulation; DNA stability, and packing, are tightly regulated *in vivo* (Cozzarelli et al., 2006; Koster et al., 2010; Lipfert et al., 2015; Liu and J.C. Wang, 1987; Luger et al., 1997; Roca, 2011; Worcel et al., 1981).

With DNA being the primary carrier of genetic information, it has long been known that RNA plays critical intermediate roles in the central dogma, facilitating the transformation of genetic information into proteins as messenger-, transfer-, and ribosomal RNA. In addition to these traditional roles, it has become increasingly clear that RNA assumes many more functions in the regulation of gene expression through mechanisms such as (self-) splicing (Cech, 1990), riboswitches (Winkler and Breaker, 2005), RNA interference (Fire et al., 1998), and the CRISPR/Cas pathway (Jinek et al., 2012; Rutkauskas et al., 2015). In these contexts, too, the physical properties of RNAs play critical roles in their folding into functional structures and their dynamics and interactions (Alexander et al., 2010; G. Lee et al., 2012; Schuwirth et al., 2005; Tama et al., 2003). Importantly, like in the case of DNA, the functional units *in vivo* often consist of both nucleic acids and proteins in tightly interacting nucleo-protein complexes.

Finally, in addition to their evolved biological roles, nucleic acids are emerging as construction materials in self-assembling nanostructures, notably as DNA and RNA "origami" structures of increasing sophistication and functionality (Castro et al., 2011; Delebecque et al., 2011; Gerling et al., 2015; Kuzyk et al., 2012; Langecker et al., 2012; Rothemund, 2006).

* Corresponding author.
E-mail address: Jan.Lipfert@lmu.de (J. Lipfert).
[1] Present address: Cavendish Laboratory, University of Cambridge, Cambridge CB3 0HE, UK.

http://dx.doi.org/10.1016/j.jsb.2016.06.022
1047-8477/

Magnetic tweezers (MT) are emerging as powerful tools to investigate the mechanical properties, conformational transitions, interactions and processing of nucleic acids at the single-molecule level (Chiou et al., 2006; Dulin et al., 2013, 2015a; Gosse and Croquette, 2002; Haber and Wirtz, 2000; Neuman and Nagy, 2008). In particular, the advent of novel kinds of magnetic tweezers that allow us to directly observe torque and twist (Celedon et al., 2009; Forth et al., 2013; Janssen et al., 2012; Kauert et al., 2011; Lebel et al., 2014; Lipfert et al., 2010a, 2011b; Mosconi et al., 2011) at the level of individual molecules provides new insights and new perspectives of the fundamental properties of nucleic acids and their interactions with proteins.

In this review, we will first summarize and highlight recent developments in magnetic tweezers. We then go on to discuss applications, first to the properties of "bare" nucleic acids, where we emphasize the many similarities but also striking differences between DNA and RNA. Finally, we highlight recent applications to the study of small molecule binding to DNA and nucleic acid-protein interactions.

2. Magnetic tweezers instruments

2.1. The principle of a magnetic tweezers setup

In magnetic tweezers (MT), the molecules of interest are tethered between a flow cell surface and magnetic beads. Typically, an inverted microscope and monochromatic illumination are used to track the diffraction pattern of the beads using video microscopy to determine their *X*, *Y*, and *Z* positions. Permanent (and in some cases electro-) magnets placed above the flow cell apply magnetic fields and thus magnetic forces and torques on the beads, which, in turn, allow stretching and twisting the molecules of interest.

2.2. Conventional magnetic tweezers

Conventional MT, pioneered by Croquette and coworkers (Strick et al., 1996), typically use pairs of cubic permanent magnets that produce a horizontal magnetic field at the location of the magnetic beads (Fig. 1a, f). This MT configuration can apply precisely calibrated forces (Gosse and Croquette, 2002; Lansdorp and Saleh, 2012; Lipfert et al., 2009; Yu et al., 2014) by controlling the distance between the magnets and the tethered beads, enabling force-extension measurements over a large range of forces, in particular also in the low force regime (<0.1 pN). In addition, due to the horizontal magnetic field (Fig. 1f), the preferred magnetization axis of the bead (van Oene et al., 2015) tightly aligns with the field, strongly confining the rotational motion of the bead. Consequently, the rotation angle of the bead barely deviates from its equilibrium position, allowing the application of precisely controlled twist to nucleic acid tethers. However, it is difficult to reliably detect angular changes and to measure torque in this conformation, which is the main difference to freely orbiting MT (FOMT) and magnetic torque tweezers (MTT), see Table 2.

2.3. Freely orbiting magnetic tweezers and the rotor bead assay

In contrast to conventional MT, freely orbiting MT (FOMT) employ cylindrical magnets (Fig. 1c) that produce a vertical field, along the tether axis. Consequently, the bead's preferred magnetization axis aligns vertically and the rotation of the bead about the tether axis is unconstrained, while there is still a controlled upward force applied to the bead that stretches the molecule. When the vertical magnet is well aligned, the bead's fluctuations in the *XY*-plane trace out a doughnut shape (Fig. 1g) and the free rotation of the bead is only constrained by the nucleic acid tether. The doughnut-shaped fluctuation pattern of the bead's motion allows the tracking of angular changes by converting the *XY*-position to radial and angular coordinates (Lipfert et al., 2011b). A conceptually similar measurement strategy is the rotor bead assay (Fig. 1b) that employs conventional magnetic tweezers to apply stretching forces and an additional fluorescent marker bead or gold nanorod in the middle of the DNA tether for angular tracking (Bryant et al., 2003; Gore et al., 2006b; Lebel et al., 2014; Oberstrass et al., 2012). Separating force actuation from angular tracking makes the rotor bead assay somewhat more complicated in terms of the molecular assembly than the FOMT (necessitating e.g. three attachment points for beads or other actuators, instead of two in the FOMT), yet has the advantage of providing greater flexibility in terms of the angular tracking approach and in particular enabling the use of very small particles for angular tracking, which increases the temporal resolution (Lebel et al., 2014).

2.4. Magnetic torque tweezers

Magnetic torque tweezers (MTT) control the rotation of the magnetic beads and thus the twist of the tethered molecule, similar to conventional MT; however, they expand the capabilities of MT by enabling direct measurements of single molecule torques (Celedon et al., 2009; Kauert et al., 2011; Lipfert et al., 2010a; Mosconi et al., 2011). The employed magnet configuration is typically similar to FOMT, with a central vertically aligned magnet. Unlike in FOMT, additional horizontal magnetic fields, either from misalignment of the central magnet (Celedon et al., 2009; Kauert et al., 2011), Helmholtz coils around the cylindrical magnet (Janssen et al., 2012), or through the use of a permanent side magnet (Lipfert et al., 2010a) (Fig. 1d, e), give rise to a weak angular trap that enables torque measurements (Fig. 1h). The horizontal field component constrains the rotation of the bead, giving rise to an arc-shape pattern in the *XY*-plane (Fig. 1h), and allows inducing twist in the molecule and measuring the restoring torque (Celedon et al., 2009; Janssen et al., 2012; Kauert et al., 2011; Lipfert et al., 2010a; Mosconi et al., 2011).

2.5. Angular tracking and the principle of torque measurements in MTT

Torque measurements in MTT rely on angular tracking to detect the rotation angle of the bead about the tether axis. Fig. 2a shows a schematic of how angular tracking in MTT enables torque measurements. At zero turns the bead is at its rotational equilibrium position Θ_0 and the nucleic acid tether is torsionally relaxed. After applying N turns the molecule is twisted and the bead's angular position is shifted (slightly) from Θ_0 to Θ_N. This change in the mean rotation angle is detectable in MTT (Fig. 2a, histograms) and provides information about the restoring torque exerted by the nucleic acid when twisting it: the molecular torque Γ_{mol} is simply given by the change in the mean rotation angle after N turns multiplied by the angular trap stiffness (k_Θ), which is in turn calibrated from the width of the thermal fluctuations (where k_BT is the thermal energy) of the bead's motion:

$$\Gamma_{mol} = -k_\Theta < \Theta_N - \Theta_0 > \text{ and } k_\Theta = k_BT/\mathrm{Var}(\Theta)$$

Several techniques have been used for angular tracking. One approach is to use cylindrical magnets plus a nanorod to which the magnetic particle is attached or two coupled magnetic beads (Fig. 1e, inset) in order to twist the molecule (Celedon et al., 2009; Mosconi et al., 2011). Additional options are to add a small fiducial marker bead to the magnetic bead (Fig. 1e and f) (Lipfert et al., 2010a) or to track intrinsic inhomogeneities of the beads (Janssen et al., 2008; Kauert et al., 2011). Finally, the

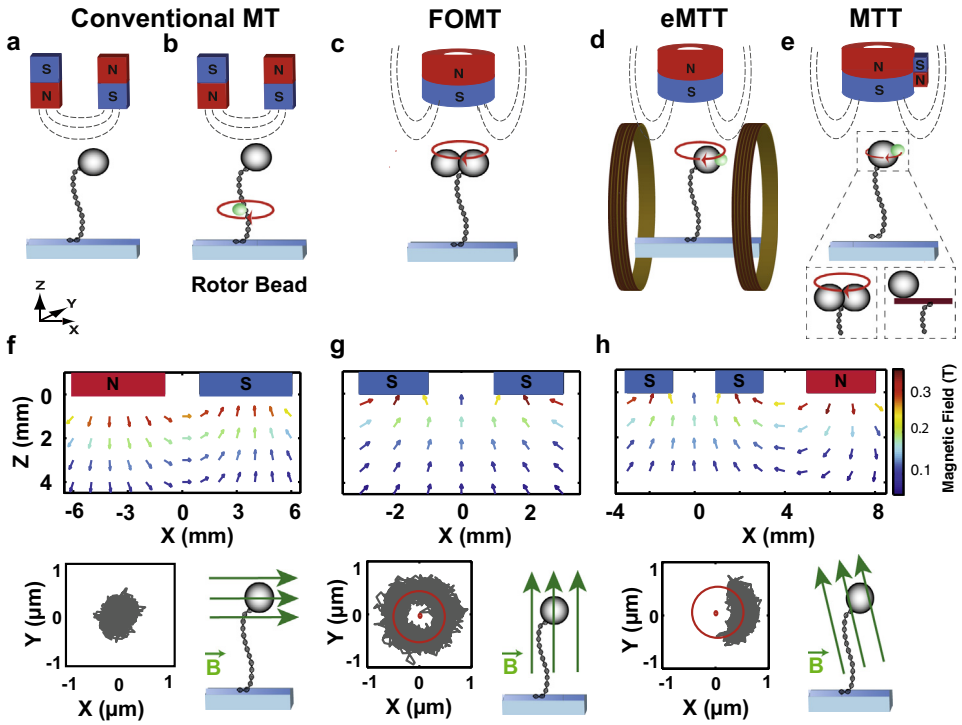

Fig. 1. Variations of magnetic tweezers (a–e). Conventional MT consist of two cubic, permanent magnets (a, b) that produce a horizontal magnetic field (f) at the location of the magnetic bead, while cylindrical magnets (c–e) create a vertical magnetic field (g). Helmholtz coils around the cylindrical magnets (d), as in electromagnetic torque tweezers (eMTT), or an additional side magnet (e), in magnetic torque tweezers (MTT), slightly tilt the vertical magnetic field (h). The *XY*-fluctuations of the magnetic bead depend strongly on the direction of the magnetic field. The rotation of the bead about the tether axis in (f) is strongly confined and deviates barely from its equilibrium position. This stands in contrast with (g), where the rotation of the bead about the tether axis is completely unconstrained and the bead's fluctuations trace out a doughnut-like shape in the *XY*-plane. In (e) MTT, with a slightly tilted magnetic field (h), the rotation of the bead is weakly confined such that the bead does not trace out a whole circle, but an arc. The field gradients in all MT configurations shown generate (upward) pulling forces on the magnetic beads, thus stretching the molecules of interest.

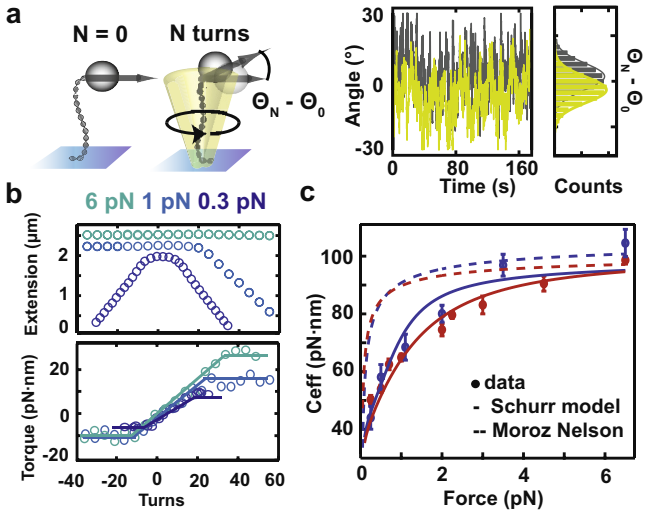

Fig. 2. Angular tracking in MT and the torque response of dsDNA. (a) When turning the magnet and thus the beads, twist is induced in the molecule that can be measured in MTT, based on detecting changes in the rotational angle. (b) Typical extension-rotation curves for dsDNA (top) showing the extension of the DNA molecule against turns at three different forces (6 pN, 1 pN, and 0.3 pN). Also shown are the corresponding torque responses of dsDNA for the three forces (bottom). (c) The torsional stiffness (C_{eff}) of dsDNA (blue; data from (Lipfert et al., 2010a)) and dsRNA (red; data from (Lipfert et al., 2014)) is force-dependent. Two models are shown: the Moroz-Nelson theory (first-order) fit to the high force data ($F > 3$ pN; dashed line) and the Schurr model (solid line), see main text for a description of the models.

experimentally most straightforward approach to angular tracking is to convert the *XY*-position to an angle for beads that move on a circular arc (Fig. 1h, bottom).

3. Applications of magnetic tweezers

3.1. The "standard model" of double-stranded DNA and RNA: nucleic acids as isotropic elastic rods

Both double-stranded DNA (dsDNA) and double-stranded RNA (dsRNA) form right-handed helices under physiological conditions, of overall similar dimensions. dsDNA naturally adopts a B-form helix, with a radius of ~1 nm, a rise per base pair of 3.4 Å (Wing et al., 1980) and a helical pitch of 10.5 base pairs per turn (Rhodes and Klug, 1980), while dsRNA takes on an A-form helix, which is somewhat shorter (2.8 Å/bp and 13 bp/turn (Taylor et al., 1985)) and thicker (~1.2 nm radius). On scales significantly larger than one base pair, double-stranded nucleic acids can be well approximated as isotropic elastic rods, at least under not too large forces and torques. An isotropic elastic rod can undergo bending, stretching and twisting deformations and its elastic response is characterized by the elastic parameters bending persistence length (A), stretch (or Young's) modulus (S), torsional persistence length (C) and twist-stretch coupling (D) (Nelson, 2002).

In recent years, all four elastic parameters were quantitatively determined for both dsDNA and dsRNA in a series of landmark single-molecule measurements, not least using a number of ingenious MT-based assays. In the next sections, we will briefly describe how the various elastic parameters have been determined. In particular, we will focus on the similarities (as might

be naively expected from their similar overall structure) yet also important differences between dsDNA and dsRNA.

3.1.1. Bending persistence length A

For forces ⩽ 10 pN, the measured force-extension response of nucleic acids is in excellent agreement with the (inextensible) worm-like chain (WLC) model of purely entropic stretching elasticity (Abels et al., 2005; Bustamante et al., 1994; Lipfert et al., 2014; Marko and Siggia, 1995). The bending persistence length *A* for both dsDNA and dsRNA has been determined from fits of the WLC model to low-force force-extension data to be ∼45 nm for dsDNA (Baumann and Smith, 1997; Bouchiat et al., 1999; Herrero-Galán et al., 2013; Lipfert et al., 2014; Wenner et al., 2002) and ∼57 nm for dsRNA (Herrero-Galán et al., 2013; Lipfert et al., 2014), in ∼150 mM monovalent salt. *A* increases strongly for low salt (<150 mM monovalent salt) whereas it decreases only slightly with increasing ionic strength (>150 mM monovalent salt) of the solution (Baumann and Smith, 1997; Wenner et al., 2002), in approximate agreement with models that split *A* into an intrinsic and an electrostatic component, first introduced independently by Odijk and Skolnick-Fixman (OSF) (Odijk, 1977; Skolnick and Fixman, 1977).

However, open questions, which are beyond the focus of this review, remain: first, the detailed dependence of the persistence length on salt concentration for multi-valent ions that are not well described in the linearized Debye-Hückel theory employed by OSF (Baumann et al., 2000; Brunet et al., 2015). Second, the treatment of flexible polymers, in particular single-stranded nucleic acids (McIntosh and Saleh, 2011; Murphy et al., 2004; Saleh et al., 2009; Sim et al., 2012), as the OSF model is strictly valid only in the stiff rod limit. Third, to what extent the other elastic parameters (in particular *C* and *D* discussed below) depend on salt.

3.1.2. Stretch modulus S

At forces ⩾ 10 pN, enthalpic contributions to the stretching response need to be taken into account and force-extension data for both dsDNA and dsRNA are well-described by the extensible WLC model that incorporates the stretch modulus *S* (Bouchiat et al., 1999; Odijk, 1995) up to forces ⩽ 50 pN, where they undergo an overstretching transition, see below. Experiments showed that the stretching modulus of dsRNA (∼350 pN) is approximately three times lower compared to that of dsDNA (∼1000 pN) (Baumann and Smith, 1997; Herrero-Galán et al., 2013; Lipfert et al., 2014; Smith et al., 1996; Wenner et al., 2002). This difference between dsDNA and dsRNA can be understood from the "springiness" of the dsRNA helix, where the bases have an inclination and for which the center line (the line connecting the centers of the base pairs) forms itself a helix, unlike for dsDNA, where the center line is almost straight (Chou et al., 2014).

3.1.3. Torsional persistence length C

Probing the torsional degrees of freedom (e.g. the elastic parameters *C* and *D*) requires single molecule methods capable of applying both forces and torques. MTT are ideally suited for this task, as they allow inducing and directly measuring torque. A typical torque measurement is shown in Fig. 2b, where both the tether extension (top) and torque (bottom) are monitored as a function of the applied turns for dsDNA, at three forces, 6 pN, 1 pN and 0.3 pN. When twisting nucleic acids close to zero turns (which corresponds to the torisonally relaxed helix) there is little change in the measured extension while the torque increases linearly with applied turns. From the slope of the torque vs. turns response in the linear regime (Fig. 2b, solid line) the effective torsional stiffness (C_{eff}) of the molecule can be determined using $C_{eff} = L_C/(2\pi N k_B T)\cdot \Gamma_{mol}$, where L_C is the contour length of the nucleic acid and *N* the applied number of turns. The effective torsional stiffness C_{eff} increases with force for both dsDNA (blue) and dsRNA (red) (Fig. 2c). This force dependence needs to be taken into account when comparing measurements *of* C_{eff} that employ measurement modalities at different forces, such as MTT, FOMT, the rotor bead assay, and fluorescence polarization anisotropy (Bryant et al., 2003; Fujimoto and Schurr, 1990; Heath et al., 1996; Lipfert et al., 2010a, 2011b; Mosconi et al., 2009; Selvin et al., 1992). Moroz and Nelson (MN) have introduced a model that rationalizes why the effective twist rigidity (C_{eff}) is smaller than the microscopic rigidity (*C*), based on the coupling of twist and bend fluctuations, and their model allows estimating *C* from rotation-extension curves (Moroz and Nelson, 1997, 1998). The MN model (Fig. 2c, dashed line) provides a reasonable description of C_{eff} as a function of force, in particular if higher order terms are included in the model (Lipfert et al., 2011b) and if the torsional persistence length is treated as a free fitting parameter (Kauert et al., 2011; Mosconi et al., 2009; Oberstrass et al., 2012). However, direct measurements of C_{eff} are not fully consistent with the MN predictions and reveal small, but systematic and statistically significant deviations between data and model. Fitting the MN model to the high force data, the measured values for C_{eff} at low forces (<1–2 pN) systematically fall below the prediction of the MN model (Lepage et al., 2015; Lipfert et al., 2010a, 2011b). To account for these deviations, Schurr has recently proposed an extension of the MN model that incorporates two different (sub-) states of the dsDNA helix and provides a closer agreement with the experimentally observed data (Fig. 2c, solid line) (Schurr, 2015). The Schurr model assumes that there are two states of the helix, which can interconvert in a cooperative fashion and differ slightly in their local rise per base pair and in their torsional rigidity. Such a two-state model was previously invoked to explain anomalous fluctuations of dsDNA in X-ray scattering measurements (Mathew-Fenn et al., 2008). Increasing the force shifts the equilibrium of the two states to the longer and torsionally stiffer sub-state. The model features a total of five fitting parameters: the equilibrium free energy difference between the two-states, a parameter associated with the cooperativity of the transition, the difference in rise per base pair between the two states, and the torsional stiffnesses of the two substates. The first three parameters are obtained from a fit to small deviations from the WLC model in force-extension data and provide the relative populations of the two states as a function of force. Finally, the torsional stiffnesses of the sub-states are fitted to the C_{eff} vs. force data. Schurr obtained values of 100 nm for the rigidity in the sub-state that is valid for high forces and 40 nm for the sub-state for low forces (for dsDNA). Those fit parameters provide a significantly better fit to the dsDNA data ($\chi^2 \sim 2$) than the original MN model ($\chi^2 \sim 13$, for a fit of the MN model over the entire force range). While the Schurr model is speculative at this time, we note that employing a similar fitting procedure, we also find a significantly improved fit to the C_{eff} vs. force data for dsRNA (Fig. 2c, red solid line, $\chi^2 \sim 6$ vs. $\chi^2 \sim 67$ where both models are fit over the entire force range), which suggests that a similar two state transition might occur in the RNA helix. Nonetheless, the introduction of two sub-states is currently somewhat *ad hoc* and further evidence (e.g. from spectroscopy) is required to test and evaluate the model.

3.1.4. The twist- stretch coupling D

The only coupling term between elastic deformations in the isotropic elastic rod model is the twist-stretch coupling constant *D*. Unlike the other elastic constants (*A*, *S*, and *C*), *D* can be both positive and negative: positive values of *D* correspond to a situation where the rod shortens upon overwinding (or, equivalently, unwinds upon stretching); negative *D* means that the rod lengthens upon overwinding (or overwinds upon stretching). Macroscopic intuition (e.g. with wringing out a towel) suggests

that overwinding should result in shortening, a behavior initially also suggested for DNA (Kamien et al., 1997; Marko, 1997). However, later high-resolution single molecule measurements revealed that, surprisingly, overwinding DNA close to its equilibrium conformation results in lengthening of the molecule (Gore et al., 2006a; Lionnet et al., 2006). Similar measurements on RNA revealed yet another surprise: RNA shortens when overwound (Lipfert et al., 2014), i.e. the twist-stretch couplings for DNA and RNA has opposite signs (Fig. 3a), a finding that challenged existing models of nucleic acid mechanics. Several generations of models have been proposed to explain the observed twist-stretch coupling: initial models treating DNA (or RNA) as an elastic medium with a helicity predict both molecules to shorten upon overwinding (Kamien et al., 1997; Marko, 1997), in disagreement with high-resolution DNA measurements. Models featuring a stiff helical backbone around a softer elastic core correctly predict the behavior for DNA, but fail for RNA (Gore et al., 2006a; Olsen and Bohr, 2011). Similarly, a modeling approach that represents DNA and RNA at the base pair level and uses available crystal structures to determine their elastic parameters ("HelixMC") correctly predicts the twist-stretch coupling for DNA, but fails for RNA (Chou et al., 2014; Lipfert et al., 2014). Conversely, a simulation framework that coarse grains DNA and RNA at the single base level ("oxRNA/oxDNA") correctly predicts the twist-stretch for RNA, but fails for DNA (Matek et al., 2015a, 2015b). A correct prediction of the puzzling difference between DNA and RNA has finally been achieved using all-atom, explicit solvent molecular dynamics simulations (Liebl et al., 2015). The molecular dynamics simulations have revealed that an increase in the inclination of bases upon overtwisting leads to a reduction in the helix radius and thus an overall extension of DNA (Fig. 3a, blue). In contrast, for RNA the bases already exhibit significant inclination in the torsionally relaxed state; overwinding thus leaves the helix' radius approximately constant and leads to shortening of the molecule (Fig. 3a, red) (Liebl et al., 2015). In summary, while being a relatively small effect, the twist-stretch coupling provides a compelling example how precision single-molecule measurements can provide stringent tests of current models of nucleic acid structure and dynamics.

3.2. Conformational transitions induced by forces and torques

In physiological conditions and in the absence of large external forces and torques, dsDNA and dsRNA adopt B-form and A-form helix structures, respectively, with elastic properties described in detail in the above sections. However, under external forces and torques both nucleic acids can undergo conformational changes

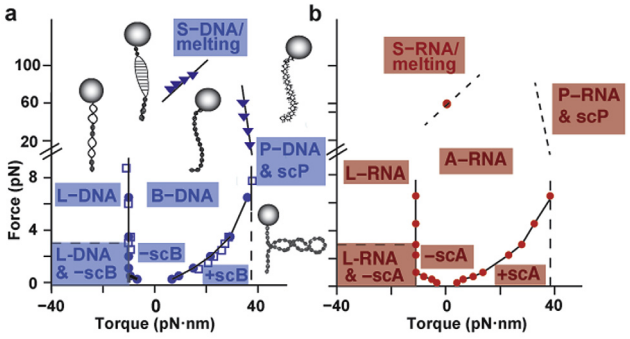

Fig. 4. Phase diagrams for dsDNA (a) and dsRNA (b). Experimentally measured critical torques and forces are indicated by symbols. Solid lines are phase boundaries that have been mapped out by direct measurements. Dashed lines are phase boundaries that are inferred from the data. The overall phase diagrams under applied forces and torques are similar for dsDNA and dsRNA. Insets in panel (a) show illustrations of the nucleic acid conformations associated with the various phases. For a detailed description of the structures and transitions see the main text. Data points for dsRNA (red dots) are from (Lipfert et al., 2014). For dsDNA, blue dots are from (Lipfert et al., 2010a), blue squares from (Sheinin et al., 2011) and blue triangles from (Bryant et al., 2003).

and take on various structural forms. Using single-molecule measurements, MT in particular, the force and torque responses of both dsDNA and dsRNA have been mapped out carefully, resulting in an (almost) complete description of the structural transitions in a force-torque phase diagram, see Fig. 4a for dsDNA and Fig. 4b for dsRNA.

3.2.1. Buckling transitions, the formation of plectonemes, and torque induced melting

When over- and underwound at relatively low forces, both dsDNA and dsRNA eventually release torsional stress by undergoing buckling transitions, resulting in the formation of plectonemic supercoils (Fig. 2b). At low forces (<1 pN), the response to positive (overwinding the helix) and negative twist (underwinding the helix) is symmetric and both dsDNA and dsRNA release torsional stress by forming positive and negative plectonemic supercoils upon over- and underwinding, respectively (see e.g. Fig. 2b, lower curves). At higher forces (>1 pN), the response upon over- and underwinding becomes asymmetric: while the molecules still buckle and form plectonemes upon overwinding, underwinding leads to torque-induced melting. The critical torques for torque-induced melting have been determined to be -10 ± 1 pN·nm for dsDNA (Bryant et al., 2003; Lipfert et al., 2010a; Sheinin et al., 2011) and -11 ± 1 pN·nm for dsRNA (Lipfert et al., 2014),

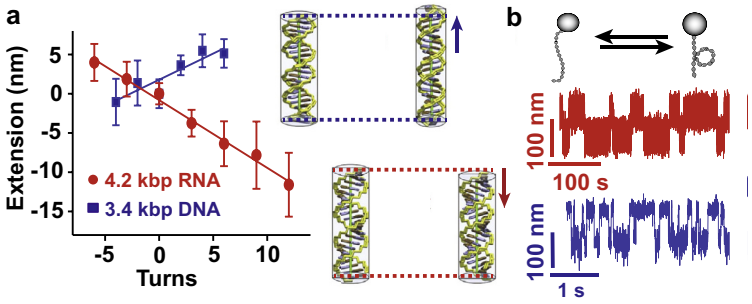

Fig. 3. Surprising differences between dsDNA (red) and dsRNA (blue). (a) Relative change in extension vs. number of applied turns for both dsDNA and dsRNA at high force (F = 7 pN). The data reveal opposite signs for the twist-stretch coupling D (Lipfert et al., 2014). The insets show the results of all atom molecular dynamics simulations (Liebl et al., 2015): DNA lengthens when overwound whereas RNA shortens, in agreement with the experimental data. (b) Extension vs. time traces for dsDNA and dsRNA at the buckling transition. The traces reveal thermally activated transitions between a twisted, but straight and a plectonemic state. The time scale for this transition is in the millisecond range for dsDNA and on the order of seconds for dsRNA under otherwise identical conditions (F = 4 pN and 320 mM NaCl).

consistent with their similar base pairing energies. The critical torques and the critical supercoiling densities for buckling are very similar for both dsDNA and dsRNA (Lipfert et al., 2014) and reasonably well described by the simple isotropic elastic rod picture (Lipfert et al., 2010a, 2014; Marko, 2007; Strick et al., 2000) and captured by coarse grained simulations (Lepage et al., 2015; Schöpflin et al., 2012).

Nonetheless, open questions remain. It is generally observed that there is a linear relationship between effective tether extension and the number of applied turns past the buckling transition, where every additional turn leads to the formation of an additional coil of the plectonemes (Lepage et al., 2015; Maffeo et al., 2010; Marko, 2007; Marko and Neukirch, 2012; Schöpflin et al., 2012). In this plectonemic regime, the torque is typically assumed to be constant and equal to the buckling torque (Marko, 2007; Mosconi et al., 2011; Strick et al., 2000), as indicated by the currently available experimental data (Celedon et al., 2009; Janssen et al., 2012; Lipfert et al., 2010a) (Fig. 2b). However, there are theoretical predictions that in the multiplectoneme regime, which will be populated particularly at low force under low salt concentrations (van Loenhout et al., 2012a), the torque will vary even in the plectonemic regime (Emanuel et al., 2013; Lepage et al., 2015; Marko and Neukirch, 2012; Schöpflin et al., 2012).

Another open question concerns the transition dynamics: a large difference was observed in the dynamics of the buckling transition from torsionally strained, but uncoiled B-DNA/A-RNA to plectonemic nucleic acids (scB-DNA/scA-RNA). The transition at the buckling point is at least two orders of magnitude faster for dsDNA than for dsRNA, see Fig. 3b (Lipfert et al., 2014).

3.2.2. Formation of P-DNA and P-RNA upon overwinding

If dsDNA or dsRNA molecules are overwound at stretching forces $\geqslant$ 5 pN, which are sufficient to suppress buckling until positive torque values of $\geqslant$35 pN·nm are reached (Bryant et al., 2003; Lipfert et al., 2010a, 2014; Sheinin and M.D. Wang, 2009) a structural transition from B-DNA to P-DNA (A-RNA to P-RNA) occurs (see schematic in Fig. 4). Both DNA and RNA P-form helices are proposed to adopt conformations with the bases facing outward and the highly overwound sugar phosphate backbone in the center (Fig. 4a, insets) (Allemand et al., 1998; Wereszczynski and Andricioaei, 2006). This is similar to the conformations that Linus Pauling (incorrectly) proposed for the equilibrium structure of dsDNA in 1953 (Pauling and Corey, 1953), hence the term "P"-DNA, and, by analogy, P-RNA. For P-DNA it is known that it has a much smaller helical twist than the B-form, experimental values range between 2.6 (Allemand et al., 1998) and 2.7 (Bryant et al., 2003) base pairs per turn. The contour length was found to be 1.5 (Bryant et al., 2003) and 1.6 times longer (Allemand et al., 1998) than B-DNA. A measured bending persistence length of 19 nm (Allemand et al., 1998) and torsional persistence length of P-DNA of 20 ± 10 nm (Marko and Neukirch, 2013) suggest P-DNA to be significantly more flexible than B-DNA. At forces < 20 pN measurements showed that there is almost no change in the extension of the nucleic acids upon overwinding into the P-form regime, which is interpreted as a transition from B-/A- to a supercoiled P-form. Above 20 pN, an increase of the molecule in length as it is overwound was observed, suggesting an extended P-form. The higher the applied force the less torque is needed to drive the transition from B to P (Bryant et al., 2003; Marko and Neukirch, 2013) (Fig. 4a).

3.2.3. Formation of L-DNA and L-RNA upon underwinding

Upon underwinding of dsDNA and dsRNA the formation of negative supercoiled plectonemes is favored up to a critical torque of −10 ± 1 pN·nm and −11 ± 1 pN·nm for dsDNA and dsRNA, respectively. At forces $\geqslant$ 1 pN (with the exact force depending on salt concentrations, temperature and pH) (Galburt et al., 2014; Salerno et al., 2012; Tempestini et al., 2013) underwinding reaches torque values sufficient to induce (partial) melting of the double-stranded helices. Upon adding more twist beyond the onset of the melting transition, the torque stays constant at the melting torque value over a large range of turns, up to a supercoiling density of −1.8 for dsDNA (Sheinin et al., 2011) and −1.9 for dsRNA (Lipfert et al., 2014), when, finally, a transition from the B-/A- to the L-form with an averaged left-handed twist takes place. The helical twist for both L-DNA and L-RNA was determined to be approximately −13 bp per turn (Lipfert et al., 2014; Sheinin et al., 2011). Compared to B-form DNA, the contour length was found to be 1.4 times larger, the bending persistence length 3 nm and the torsional stiffness 10–20 nm (Sheinin et al., 2011).

A more detailed analysis whether the L-form consists of melted base pairs and/or of "Z-DNA" (a left-handed form of DNA that is slightly longer and has reverse twist (Sheinin et al., 2011; Thomas and Bloomfield, 1983)) found that in a DNA sequence featuring multiple GC-repeats underwinding induces a transition to Z-DNA at approximately −3 pN·nm; however, for a random DNA sequence no sharp transition was observed (M. Lee et al., 2010; Oberstrass et al., 2012, 2013). Taken together, these data suggest that underwound DNA under sufficiently high forces and torques features a co-existence of B-, Z-form and melted DNA.

3.2.4. Formation of S-DNA and S-RNA upon overstretching

When pulling on torsionally unconstrained dsDNA or dsRNA with forces higher than 50 pN, B-DNA and A-RNA undergo a rapid overstretching transition, suddenly lengthening by a factor of ∼1.7 and ∼1.9, respectively (Bonin et al., 2002; Cluzel et al., 1996; Herrero-Galán et al., 2013; Lipfert et al., 2014; Smith et al., 1996). The exact force at which the transition takes place is lower for dsRNA than for dsDNA (Herrero-Galán et al., 2013; Lipfert et al., 2014) and depends on ionic strength (Baumann and Smith, 1997; Smith et al., 1996; Wenner et al., 2002), temperature (Williams et al., 2001a), GC content of the nucleic acids sequence (Rief et al., 1999) and pH (Williams et al., 2001b). Two models have been proposed for the nature of this overstretched form. One model describes the molecule with elongated base pairs, stretched but still double-stranded (Cluzel et al., 1996; Smith et al., 1996), a form usually referred to as stretched or S-DNA, with (partial) melting occurring at even higher forces (Rief et al., 1999). The helical twist of S-DNA was suggested to be 35 base pairs per right-handed turn (Bryant et al., 2003; Léger et al., 1999; Sarkar et al., 2001). The other model interprets the overstretching transition as force-induced melting and breaking of the hydrogen bonds when pulling, leading to a splitting of the helix into two single-strands (van Mameren et al., 2009; Wenner et al., 2002; Williams et al., 2001a,b).

In contrast, for torsionally constrained dsDNA and dsRNA, no sharp plateau but a gradual extension of the molecule is observed (Lipfert et al., 2014; Paik and Perkins, 2011; van Mameren et al., 2009). Recent results for dsDNA suggest that both force-induced strand separation and S-DNA formation can occur, depending on sequence content, temperature, and salt concentration (Bosaeus et al., 2012; King et al., 2013; Zhang et al., 2012). Less is known about the overstretching transition for dsRNA, however, it appears plausible that similar overstretching modes exist.

An overview of experimentally determined values for the elastic properties of dsDNA and dsRNA are listed in Table 1; corresponding references are given in the text.

3.3. Interactions of nucleic acids with small-molecules and proteins

Going beyond the mechanical properties and conformational transitions of "bare" nucleic acids, MT are a powerful tool to study

Table 1
Mechanical and structural parameters of various conformations of dsDNA and dsRNA. A collection of measured values for the persistence length *A*, the torsional stiffness *C*, the helical pitch and the rise per base pair are listed for A-RNA, B-DNA, P-DNA, L-DNA, S-DNA and Z-DNA. "Relative extension" describes the contour lengths relative to the state of the nucleic acid at low forces and torques.

	A-RNA	B-DNA	P-DNA	L-DNA	S-DNA	Z-DNA
A (in nm)	57	45	19	3	15*	200
C (in nm) at high force	100	109	20 ± 10	10–20	No value available	No value available
Helical pitch (bp per turn)	13	10.5	2.6 2.7	−12 to −15	35	−12
Relative extension	1	1	1.5 1.6	1.4	1.7	1.1
Rise per bp (nm/bp)	0.28	0.34	0.54	0.48	0.58	0.37
Helicity	Right-handed	Right-handed	Right-handed	Left-handed	Right-handed	Left-handed

* This value was derived theoretically by Storm and Nelson (2003).

Table 2
Comparison of the capabilities of different MT configurations. All magnet configurations exert and allow measuring forces, generally ranging from 0.1 pN to 100 pN. Tracking in *X*, *Y* and *Z* is possible in all cases with a resolution down to 1 nm or less. Torque can be applied in conventional MT and also in MTT. In contrast to MTT, conventional MT do not allow measuring torque. In FOMT, the bead's motion is unconstrained around its tether axis and it is free to rotate. This feature can be exploited to observe angular changes.

	Conventional MT	FOMT	MTT
Force	Apply and measure	Apply and measure	Apply and measure
XYZ-tracking	Yes	Yes	Yes
Torque	Apply only	Free rotation	Apply and measure
Angle tracking	No	Yes	Yes

nucleic acid-protein and drug interactions and to dissect, e.g., the processes underlying replication, transcription, and repair of DNA and RNA, which are central to cellular and viral lifecycles. There are a number of excellent reviews of these applications of MT (Bryant et al., 2012; Dulin et al., 2013, 2015a; Forth et al., 2013; Lipfert et al., 2015; Manosas et al., 2010). Here, we highlight only briefly a few recent studies involving the twist dependence of small-molecule binding and the use of novel MT approaches such as FOMT to probe DNA-protein interactions.

3.3.1. Detecting small-molecule binding to DNA in MT

MT (and MTT (Celedon et al., 2010)) have been used to measure the effect of various small molecules binding to DNA, in particular of the intercalators ethidium bromide (EtBr) and doxorubicin (DOXO), of netropsin (a minor-groove binder), and of topotecan and cisplatin, which are used as chemotherapeutics (Lipfert et al., 2010b; Salerno et al., 2010). Intercalators generally lengthen (Cluzel et al., 1996; Krautbauer et al., 2002; Matera et al., 2007; Sischka et al., 2005; Vladescu et al., 2007) and unwind (Lipfert et al., 2010b; Salerno et al., 2010) the DNA helix, as would be expected from their binding mode where an aromatic moiety is inserted between the stacked DNA bases. The length increase per intercalation event is ~3.4 Å, i.e. inserting an aromatic moiety into the DNA helix has an effect on its length similar to adding a base pair. In the process, the helix unwinds. For ethidium bromide, the unwinding angle per intercalated molecules was found to be 27° ± 1° (Lipfert et al., 2010b), a value likely representative for other monointercalators. In contrast, it is an open question how much bis-intercalators unwind the helix. For example for YOYO-1, a frequently used bis-intercalator, literature values range from 24° to 106° unwinding per dye (Günther et al., 2010; Johansen and Jacobsen, 1998), while the naive estimate from monointercalation would suggest 2 × 27° = 54°. In addition, the fact that intercalation unwinds the helix suggests that binding of intercalators is likely to be torque dependent, which is confirmed by preliminary experiments (Celedon et al., 2010) but awaits further quantification.

In contrast to intercalators, minor groove binders have much smaller effects on either DNA length or twist. Netropsin was found to slightly overwind the helix upon binding (Lipfert et al., 2010b), but it is unclear whether this is a general effect of minor groove binding.

3.4. Investigating nucleic acid protein interactions in FOMT

FOMT are capable of detecting changes in the tether extension, and, at the same time, they allow for angle tracking (Table 2). This combination makes them particularly appealing for the study of processes that affect both the length and overall twist of the nucleic acid, e.g. upon protein binding.

3.4.1. RNA polymerase

A classic study employed a FOMT-like assay to monitor RNA polymerase transcribing DNA (Harada et al., 2001). RNA polymerase was attached to the bottom of the flow cell and a magnetic bead to a DNA molecule. With additional fluorescent markers on the magnetic bead, the rotation of the bead and thus DNA while being transcribed by the enzyme was detected. It was observed that RNA polymerase rotates DNA clockwise and that the enzyme exerts torques up to >5 pN·nm (Harada et al., 2001), in an NTP-dependent fashion. Recent studies finally indicated that RNA polymerase is able to generate upstream torques with a mean of 11.0 ± 3.7 pN·nm and downstream torques with a maximum at 10.6 ± 4.1 pN·nm, consistent with DNA melting torque (Ma et al., 2013).

3.4.2. Recombinases RecA and Rad51

More recent work exploited the ability to track tether length and rotation at the same time. Two studies investigated RecA (from bacteria) and the homologous Rad51 (from eukaryotes), which are proteins involved in the repair of DNA by homologous recombination (Candelli et al., 2013). To enable recombination, RecA or Rad51 proteins bind cooperatively and assemble as a filament on DNA, in the process lengthening and unwinding the double-helix. The assembly of RecA and RAD51 filaments on DNA can be monitored in real-time using FOMT (M. Lee et al., 2013; Lipfert et al., 2011b). The studies revealed a lengthening of 0.5 nm and an unwinding angle of ~45° per RecA or RAD51 monomer (M. Lee et al., 2013;

Lipfert et al., 2011b), in agreement with biochemical and structural evidence.

3.4.3. Nucleosomes

A similar measurement strategy was used to study the assembly and dynamics of nucleosomes on DNA. Nucleosomes consist of ~150 bp of DNA tightly wrapped around a histone core and are the basic packaging unit of DNA in the nucleus (Luger et al., 1997; Sheinin et al., 2013). Interactions of nucleosomes and their higher order assemblies in nucleosome fibers and ultimately chromosomes are critical processes for genome storage and regulation. The assembly of single nucleosomes (consisting of dimers of H2A, H2B, H3 and H4) and tetrasomes (involving only H3 and H4) was studied using FOMT, monitoring the change in extension and in linking number at the same time (Vlijm et al., 2015b). The data showed that the assembly of a single nucleosome shortens the molecule by 46 nm, which corresponds to ~146 base pairs, and induces a change in the linking number of −1.2 (Vlijm et al., 2015a). For tetrasomes the compaction in length was 24 nm and the change in twist −0.73 for the preferred, left-handed state (Vlijm et al., 2015a). Surprisingly, it was observed that tetrasomes fluctuate between a preferred left-handed state, and a right-handed conformation, separated by a linking number difference of 1.7 ± 0.1 turns, without changing the overall extension. In addition, direct torque measurements revealed that the application of weak positive torques is sufficient to drive all tetrasomes into the right-handed state (and vice versa).

3.4.4. (Reverse) Gyrase

Two final illustrative examples of studies employing FOMT-type instruments look at DNA (reverse) gyrase. The rotor bead assay was employed to probe the enzymatic activity of gyrase, which can introduce negative supercoils in DNA in an ATP-dependent fashion, e.g. to compact the genome, to relieve strain during replication, and to promote local melting (Gore et al., 2006b). Interestingly, stepwise activity was observed showing that the unwinding takes place in multiples of two. Applying forces ranging from 0.35 pN to 1.3 pN showed that the enzymatic activity is strongly inhibited with increasing forces and revealed a kinetic intermediate (Basu et al., 2012; Gore et al., 2006b).

A FOMT-like assay was used to obtain the first single-molecule characterization of reverse gyrase, an enzyme found in hyperthermophiles that can introduce positive supercoils into DNA in an ATP-dependent fashion, an activity suggested to help increase DNA stability under elevated temperatures (Ogawa et al., 2015). The single-molecule study found 5-fold higher activity than previously determined in bulk, but also revealed that relatively small forces (~0.5 pN) or torques (~5 pN·nm) abolish activity (Ogawa et al., 2015).

4. Summary

> *Yesterday's sensation is today's calibration and tomorrow's background.*
>
> [Richard Feynman]

Single-molecule measurements of DNA beautifully illustrate the famous quote by Richard Feynman (Goodstein, 2011). The first stretching experiments on DNA (Bustamante et al., 1994; Smith et al., 1992) ushered in the field of single-molecule nanomechanics; now the WLC-type stretching response of DNA is frequently used as a calibration of instruments or new techniques and, furthermore, currently the dominant source of background noise in single-molecule protein folding experiments that use DNA linkers (Hinczewski et al., 2010, 2013). Similarly, the first DNA twisting experiments in MT opened up the possibility to observe torque-induced DNA supercoiling and melting at the level of individual molecules for the first time (Strick et al., 1996, 1998). Now, the asymmetric twisting response of DNA under forces > 1 pN is routinely used to verify that magnetic beads are attached by only a single double-stranded DNA tether. In addition, high-resolution twist and torque measurements of DNA now allow us to test and to precisely calibrate models of nucleic acids (Chou et al., 2014; Emanuel et al., 2013; Liebl et al., 2015). At the same time, the intrinsic fluctuations of supercoiled DNA provide the dominant source of noise in experiments that use supercoiled DNA in MT to detect protein binding and activity; similarly, the intrinsic torsional stiffness of DNA limits the angle and time resolution in assays that employ DNA twisting for the same purpose (Lebel et al., 2014; Mosconi et al., 2011).

We anticipate that high-resolution single-molecule measurements will continue to inspire and test increasingly refined models of nucleic acid mechanics and structure. Outstanding questions in particular regarding the behavior under twist and torque are, *inter alia*, the torque in the (multi-)plectoneme regime, the discrepancy between the observed effective torsional stiffness at low forces and the predictions of the basic isotropic rod model, and the buckling dynamics of DNA and RNA. Such models form the basis of a quantitative understanding of the behavior of nucleic acids in biological contexts and of engineered nanostructures that increasingly employ DNA and RNA as building materials.

Going beyond the properties of bare nucleic acids, MT will be an invaluable tool to dissect the mechanical properties and conformational transitions of nucleo-protein complexes and filaments, which are involved in many, if not all, fundamental processes of genome processing and maintenance. Examples include nucleosomes and their higher order assemblies and various filamentous structures involved in DNA processing and repair. Finally, MT measurements will increasingly contribute to our understanding of the dynamic processes and molecular machinery at the heart of the central dogma.

New and exciting applications of MT are made possible by a number of dramatic improvements of the measurement capabilities of MT based assays in the last few years. First, the ability to directly measure torque and twist has been discussed in detail in this review. Second, improvements in camera hardware and tracking algorithms (Lipfert et al., 2011a; van Loenhout et al., 2012b) have made it possible to perform massively parallel multi bead measurements, of up to 1000 s of beads simultaneously (Cnossen et al., 2014; De Vlaminck et al., 2011; Ribeck and Saleh, 2008). Third, advances in camera hardware, GPU-based tracking, and novel approaches to illumination enable camera-based tracking at >kHz frequencies (Dulin et al., 2015b; Huhle et al., 2015; Lansdorp et al., 2013). Fourth, other technical improvements such as temperature control during MT measurements (Galburt et al., 2014; Gollnick et al., 2014), which is crucial for many biological systems, further enhance the capabilities of MT measurements. Finally, MT can be combined with other measurement modalities, such as optical tweezers (De Vlaminck et al., 2012) or fluorescence detection (Kemmerich et al., 2015; M. Lee et al., 2010; van Loenhout et al., 2012a), enabling complementary types of measurements to, e.g., dissect the mechano-chemistry of nucleic acid processing enzymes.

In conclusion, MT based measurements will continue down the path outlined in Feynman's famous quote: making new discoveries, enabling precision experiments, and pushing the limits of physical detection.

Acknowledgements

We thank Philipp Walker for sharing unpublished data on the DNA buckling transition and all members of our laboratory for

useful discussions. We acknowledge funding from the German Research Foundation (DFG) through the Nanosystems Initiative Munich (NIM) and Sonderforschungbereich SFB 863 "Forces in Biomolecular Systems". We acknowledge the tremendous research efforts by groups in the magnetic tweezers and nucleic acids communities and regret that owing to limitations of space and scope it was not possible to cite a larger number of high-quality works.

References

Abels, J.A., Moreno-Herrero, F., Van Der Heijden, T., Dekker, C., Dekker, N.H., 2005. Single-molecule measurements of the persistence length of double-stranded RNA. Biophys. J. 88, 2737–2744.
Alexander, R.W., Eargle, J., Luthey-Schulten, Z., 2010. Experimental and computational determination of tRNA dynamics. FEBS Lett. 584, 376–386.
Allemand, J.F., Bensimon, D., Lavery, R., Croquette, V., 1998. Stretched and overwound DNA forms a Pauling-like structure with exposed bases. Proc. Natl. Acad. Sci. U.S.A. 95, 14152–14157.
Basu, A., Schoeffler, A.J., Berger, J.M., Bryant, Z., 2012. ATP binding controls distinct structural transitions of *Escherichia coli* DNA gyrase in complex with DNA. Nat. Struct. Mol. Biol. 19, 538–546.
Baumann, C.G., Smith, S.B., 1997. Ionic effects on the elasticity of single DNA molecules. Proc. Natl. Acad. Sci. U.S.A.
Baumann, C.G., Bloomfield, V.A., Smith, S.B., Bustamante, C., Wang, M.D., Block, S.M., 2000. Stretching of single collapsed DNA molecules. Biophys. J. 78, 1965–1978.
Bonin, M., Zhu, R., Klaue, Y., Oberstrass, J., Oesterschulze, E., Nellen, W., 2002. Analysis of RNA flexibility by scanning force spectroscopy. Nucleic Acids Res. 30, e81.
Bosaeus, N., El-Sagheer, A.H., Brown, T., Smith, S.B., Åkerman, B., Bustamante, C., Nordén, B., 2012. Tension induces a base-paired overstretched DNA conformation. Proc. Natl. Acad. Sci. U.S.A. 109, 15179–15184.
Bouchiat, C., Wang, M.D., Allemand, J., Strick, T., Block, S.M., Croquette, V., 1999. Estimating the persistence length of a worm-like chain molecule from force-extension measurements. Biophys. J. 76, 409–413.
Brunet, A., Tardin, C., Salomé, L., Rousseau, P., Destainville, N., Manghi, M., 2015. Dependence of DNA persistence length on ionic strength of solutions with monovalent and divalent salts: a joint theory-experiment study. Macromolecules.
Bryant, Z., Stone, M.D., Gore, J., Smith, S.B., Cozzarelli, N.R., Bustamante, C., 2003. Structural transitions and elasticity from torque measurements on DNA. Nature 424, 338–341.
Bryant, Z., Oberstrass, F.C., Basu, A., 2012. Recent developments in single-molecule DNA mechanics. Curr. Opin. Struct. Biol. 22, 304–312.
Bustamante, C., Marko, J.F., Siggia, E.D., Smith, S., 1994. Entropic elasticity of lambda-phage DNA. Science 265, 1599–1600.
Candelli, A., Modesti, M., Peterman, E.J.G., Wuite, G.J.L., 2013. Single-molecule views on homologous recombination. Q. Rev. Biophys. 46, 323–348.
Castro, C.E., Kilchherr, F., Kim, D.-N., Shiao, E.L., Wauer, T., Wortmann, P., Bathe, M., Dietz, H., 2011. A primer to scaffolded DNA origami. Nat. Methods 8, 221–229.
Cech, T.R., 1990. Self-splicing of group I introns. Annu. Rev. Biochem. 59, 543–568.
Celedon, A., Nodelman, I.M., Wildt, B., Dewan, R., Searson, P., Wirtz, D., Bowman, G. D., Sun, S.X., 2009. Magnetic tweezers measurement of single molecule torque. Nano Lett. 9, 1720–1725.
Celedon, A., Wirtz, D., Sun, S., 2010. Torsional mechanics of DNA are regulated by small-molecule intercalation. J. Phys. Chem. B 114, 16929–16935.
Chiou, C.-H., Huang, Y.-Y., Chiang, M.-H., Lee, H.-H., Lee, G.-B., 2006. New magnetic tweezers for investigation of the mechanical properties of single DNA molecules. Nanotechnology 17, 1217–1224.
Chou, F.-C., Lipfert, J., Das, R., 2014. Blind predictions of DNA and RNA tweezers experiments with force and torque. PLoS Comput. Biol. 10, e1003756.
Cluzel, P., Lebrun, A., Heller, C., Lavery, R., Viovy, J.L., Chatenay, D., Caron, F., 1996. DNA: an extensible molecule. Science 271, 792–794.
Cnossen, J.P., Dulin, D., Dekker, N.H., 2014. An optimized software framework for real-time, high-throughput tracking of spherical beads. Rev. Sci. Instrum. 85, 103712.
Cozzarelli, N.R., Cost, G.J., Nöllmann, M., Viard, T., Stray, J.E., 2006. Giant proteins that move DNA: bullies of the genomic playground. Nat. Rev. Mol. Cell Biol. 7, 580–588.
De Vlaminck, I., Henighan, T., van Loenhout, M.T.J., Pfeiffer, I., Huijts, J., Kerssemakers, J.W.J., Katan, A.J., van Langen-Suurling, A., van der Drift, E., Wyman, C., Dekker, C., 2011. Highly parallel magnetic tweezers by targeted DNA tethering. Nano Lett. 11, 5489–5493.
De Vlaminck, I., van Loenhout, M.T., Zweifel, L., Blanken Den, J., Hooning, K., Hage, S., Kerssemakers, J., Dekker, C., 2012. Mechanism of homology recognition in DNA recombination from dual-molecule experiments. Mol. Cell 46, 616–624.
Delebecque, C.J., Lindner, A.B., Silver, P.A., Aldaye, F.A., 2011. Organization of intracellular reactions with rationally designed RNA assemblies. Science 333, 470–474.
Dulin, D., Lipfert, J., Moolman, M.C., Dekker, N.H., 2013. Studying genomic processes at the single-molecule level: introducing the tools and applications. Nat. Rev. Genet. 14, 9–22.
Dulin, D., Berghuis, B.A., Depken, M., Dekker, N.H., 2015a. Untangling reaction pathways through modern approaches to high-throughput single-molecule force-spectroscopy experiments. Curr. Opin. Struct. Biol. 34, 116–122.
Dulin, D., Cui, T.J., Cnossen, J., Docter, M.W., Lipfert, J., Dekker, N.H., 2015b. High spatiotemporal-resolution magnetic tweezers: calibration and applications for DNA dynamics. Biophys. J. 109, 2113–2125.
Emanuel, M., Lanzani, G., Schiessel, H., 2013. Multiplectoneme phase of double-stranded DNA under torsion. Phys. Rev. E Stat. Nonlin. Soft Matter Phys. 88, 022706.
Fire, A., Xu, S., Montgomery, M.K., Kostas, S.A., Driver, S.E., Mello, C.C., 1998. Potent and specific genetic interference by double-stranded RNA in *Caenorhabditis elegans*. Nature 391, 806–811.
Forth, S., Sheinin, M.Y., Inman, J., Wang, M.D., 2013. Torque measurement at the single-molecule level. Annu. Rev. Biophys. 42, 583–604.
Fujimoto, B.S., Schurr, J.M., 1990. Dependence of the torsional rigidity of DNA on base composition. Nature 344, 175–177.
Galburt, E.A., Tomko, E.J., Stump, W.T., Ruiz Manzano, A., 2014. Force-dependent melting of supercoiled DNA at thermophilic temperatures. Biophys. Chem. 187–188, 23–28.
Gerling, T., Wagenbauer, K.F., Neuner, A.M., Dietz, H., 2015. Dynamic DNA devices and assemblies formed by shape-complementary, non-base pairing 3D components. Science 347, 1446–1452.
Gollnick, B., Carrasco, C., Zuttion, F., Gilhooly, N.S., Dillingham, M.S., Moreno-Herrero, F., 2014. Probing DNA helicase kinetics with temperature-controlled magnetic tweezers. Small 11, 1273–1284.
Goodstein, D., 2011. Adventures of Cosmology.
Gore, J., Bryant, Z., Nöllmann, M., Le, M.U., Cozzarelli, N.R., Bustamante, C., 2006a. DNA overwinds when stretched. Nature 442, 836–839.
Gore, J., Bryant, Z., Stone, M.D., Nöllmann, M., Cozzarelli, N.R., Bustamante, C., 2006b. Mechanochemical analysis of DNA gyrase using rotor bead tracking. Nature 439, 100–104.
Gosse, C., Croquette, V., 2002. Magnetic tweezers: micromanipulation and force measurement at the molecular level. Biophys. J. 82, 3314–3329.
Günther, K., Mertig, M., Seidel, R., 2010. Mechanical and structural properties of YOYO-1 complexed DNA. Nucleic Acids Res. 38, 6526–6532.
Haber, C., Wirtz, D., 2000. Magnetic tweezers for DNA micromanipulation. Rev. Sci. Instrum. 71, 4561–4570.
Harada, Y., Ohara, O., Takatsuki, A., Itoh, H., Shimamoto, N., Kinosita, K., 2001. Direct observation of DNA rotation during transcription by *Escherichia coli* RNA polymerase. Nature 409, 113–115.
Heath, P.J., Clendenning, J.B., Fujimoto, B.S., Schurr, M.J., 1996. Effect of bending strain on the torsion elastic constant of DNA. J. Mol. Biol. 260, 718–730.
Herrero-Galán, E., Fuentes-Perez, M.E., Carrasco, C., Valpuesta, J.M., Carrascosa, J.L., Moreno-Herrero, F., Arias-Gonzalez, J.R., 2013. Mechanical identities of RNA and DNA double helices unveiled at the single-molecule level. J. Am. Chem. Soc. 135, 122–131.
Hinczewski, M., Hansen Von, Y., Netz, R.R., 2010. Deconvolution of dynamic mechanical networks. Proc. Natl. Acad. Sci. U.S.A. 107, 21493–21498.
Hinczewski, M., Gebhardt, J.C.M., Rief, M., Thirumalai, D., 2013. From mechanical folding trajectories to intrinsic energy landscapes of biopolymers. Proc. Natl. Acad. Sci. U.S.A. 110, 4500–4505.
Huhle, A., Klaue, D., Brutzer, H., Daldrop, P., Joo, S., Otto, O., Keyser, U.F., Seidel, R., 2015. Camera-based three-dimensional real-time particle tracking at kHz rates and Ångström accuracy. Nat. Commun. 6, 5885.
Janssen, X.J., Schellekens, A.J., van Ommering, K., van IJzendoorn, L.J., Prins, M.W., 2008. Controlled torque on superparamagnetic beads for functional biosensors. Biosens Bioelectron.
Janssen, X.J.A., Lipfert, J., Jager, T., Daudey, R., Beekman, J., Dekker, N.H., 2012. Electromagnetic torque tweezers: a versatile approach for measurement of single-molecule twist and torque. Nano Lett. 12, 3634–3639.
Jinek, M., Chylinski, K., Fonfara, I., Hauer, M., Doudna, J.A., Charpentier, E., 2012. A programmable dual-RNA-guided DNA endonuclease in adaptive bacterial immunity. Science 337, 816–821.
Johansen, F., Jacobsen, J.P., 1998. 1H NMR studies of the bis-intercalation of a homodimeric oxazole yellow dye in DNA oligonucleotides. J. Biomol. Struct. Dyn. 16, 205–222.
Kamien, R.D., Lubensky, T.C., Nelson, P., Ohern, C.S., 1997. Direct determination of DNA twist-stretch coupling. Europhys. Lett. 38, 237–242.
Kauert, D.J., Kurth, T., Liedl, T., Seidel, R., 2011. Direct mechanical measurements reveal the material properties of three-dimensional DNA origami. Nano Lett. 11, 5558–5563.
Kemmerich, F.E., Swoboda, M., Kauert, D.J., Grieb, M.S., Hahn, S., Schwarz, F.W., Seidel, R., Schlierf, M., 2015. Simultaneous single-molecule force and fluorescence sampling of DNA nanostructure conformations using magnetic tweezers. Nano Lett. 16, 381–386.
King, G.A., Gross, P., Bockelmann, U., Modesti, M., Wuite, G.J.L., Peterman, E.J.G., 2013. Revealing the competition between peeled ssDNA, melting bubbles, and S-DNA during DNA overstretching using fluorescence microscopy. Proc. Natl. Acad. Sci. U.S.A. 110, 3859–3864.
Koster, D.A., Crut, A., Shuman, S., Bjornsti, M.-A., Dekker, N.H., 2010. Cellular strategies for regulating DNA supercoiling: a single-molecule perspective. Cell 142, 519–530.
Krautbauer, R., Pope, L.H., Schrader, T.E., Allen, S., Gaub, H.E., 2002. Discriminating small molecule DNA binding modes by single molecule force spectroscopy. FEBS Lett. 510, 154–158.
Kuzyk, A., Schreiber, R., Fan, Z., Pardatscher, G., Roller, E.-M., Högele, A., Simmel, F.C., Govorov, A.O., Liedl, T., 2012. DNA-based self-assembly of chiral plasmonic nanostructures with tailored optical response. Nature 483, 311–314.

Langecker, M., Arnaut, V., Martin, T.G., List, J., Renner, S., Mayer, M., Dietz, H., Simmel, F.C., 2012. Synthetic lipid membrane channels formed by designed DNA nanostructures. Science 338, 932–936.
Lansdorp, B.M., Saleh, O.A., 2012. Power spectrum and Allan variance methods for calibrating single-molecule video-tracking instruments. Rev. Sci. Instrum. 83, 025115.
Lansdorp, B.M., Tabrizi, S.J., Dittmore, A., Saleh, O.A., 2013. A high-speed magnetic tweezer beyond 10,000 frames per second. Rev. Sci. Instrum. 84, 044301.
Lebel, P., Basu, A., Oberstrass, F.C., Tretter, E.M., Bryant, Z., 2014. Gold rotor bead tracking for high-speed measurements of DNA twist, torque and extension. Nat. Methods 11, 456–462.
Lee, M., Kim, S.H., Hong, S.-C., 2010. Minute negative superhelicity is sufficient to induce the B–Z transition in the presence of low tension. Proc. Natl. Acad. Sci. U. S.A. 107, 4985–4990.
Lee, G., Bratkowski, M.A., Ding, F., Ke, A., Ha, T., 2012. Elastic coupling between RNA degradation and unwinding by an exoribonuclease. Science 336, 1726–1729.
Lee, M., Lipfert, J., Sanchez, H., Wyman, C., Dekker, N.H., 2013. Structural and torsional properties of the RAD51-dsDNA nucleoprotein filament. Nucleic Acids Res. 41, 7023–7030.
Léger, J.F., Romano, G., Sarkar, A., Robert, J., Bourdieu, L., Chatenay, D., Marko, J.F., 1999. Structural transitions of a twisted and stretched DNA molecule. Phys. Rev. Lett. 83, 1066–1069.
Lepage, T., Képès, F., Junier, I., 2015. Thermodynamics of long supercoiled molecules: insights from highly efficient Monte Carlo simulations. Biophys. J. 109, 135–143.
Liebl, K., Drsata, T., Lankas, F., Lipfert, J., Zacharias, M., 2015. Explaining the striking difference in twist-stretch coupling between DNA and RNA: a comparative molecular dynamics analysis. Nucleic Acids Res. 43, 10143–10156.
Lionnet, T., Joubaud, S., Lavery, R., Bensimon, D., Croquette, V., 2006. Wringing out DNA. Phys. Rev. Lett. 96, 178102.
Lipfert, J., Hao, X., Dekker, N.H., 2009. Quantitative modeling and optimization of magnetic tweezers. Biophys. J. 96, 5040–5049.
Lipfert, J., Kerssemakers, J.W.J., Jager, T., Dekker, N.H., 2010a. Magnetic torque tweezers: measuring torsional stiffness in DNA and RecA-DNA filaments. Nat. Methods 7, 977–980.
Lipfert, J., Klijnhout, S., Dekker, N.H., 2010b. Torsional sensing of small-molecule binding using magnetic tweezers. Nucleic Acids Res. 38, 7122–7132.
Lipfert, J., Kerssemakers, J.J.W., Rojer, M., Dekker, N.H., 2011a. A method to track rotational motion for use in single-molecule biophysics. Rev. Sci. Instrum. 82, 103707.
Lipfert, J., Wiggin, M., Kerssemakers, J.W.J., Pedaci, F., Dekker, N.H., 2011b. Freely orbiting magnetic tweezers to directly monitor changes in the twist of nucleic acids. Nat. Commun. 2, 439-9.
Lipfert, J., Skinner, G.M., Keegstra, J.M., Hensgens, T., Jager, T., Dulin, D., Köber, M., Yu, Z., Donkers, S.P., Chou, F.-C., Das, R., Dekker, N.H., 2014. Double-stranded RNA under force and torque: similarities to and striking differences from double-stranded DNA. Proc. Natl. Acad. Sci. U.S.A. 111, 15408–15413.
Lipfert, J., van Oene, M.M., Lee, M., Pedaci, F., Dekker, N.H., 2015. Torque spectroscopy for the study of rotary motion in biological systems. Chem. Rev. 115, 1449–1474.
Liu, L.F., Wang, J.C., 1987. Supercoiling of the DNA template during transcription. Proc. Natl. Acad. Sci. U.S.A. 84, 7024–7027.
Luger, K., Mäder, A.W., Richmond, R.K., Sargent, D.F., Richmond, T.J., 1997. Crystal structure of the nucleosome core particle at 2.8 A resolution. Nature 389, 251–260.
Ma, J., Bai, L., Wang, M.D., 2013. Transcription under torsion. Science 340, 1580–1583.
Maffeo, C., Schöpflin, R., Brutzer, H., Stehr, R., Aksimentiev, A., Wedemann, G., Seidel, R., 2010. DNA–DNA interactions in tight supercoils are described by a small effective charge density. Phys. Rev. Lett. 105, 158101–158104.
Manosas, M., Meglio, A., Spiering, M.M., Ding, F., Benkovic, S.J., Barre, F.-X., Saleh, O. A., Allemand, J.F., Bensimon, D., Croquette, V., 2010. Magnetic tweezers for the study of DNA tracking motors. Methods Enzymol. 475, 297–320.
Marko, J.F., 1997. Stretching must twist DNA. Europhys. Lett. 38, 183–188.
Marko, J.F., 2007. Torque and dynamics of linking number relaxation in stretched supercoiled DNA. Phys. Rev. E Stat. Nonlin. Soft Matter Phys. 76, 021926.
Marko, J.F., Neukirch, S., 2012. Competition between curls and plectonemes near the buckling transition of stretched supercoiled DNA. Phys. Rev. E Stat. Nonlin. Soft Matter Phys. 85, 011908.
Marko, J.F., Neukirch, S., 2013. Global force-torque phase diagram for the DNA double helix: structural transitions, triple points, and collapsed plectonemes. Phys. Rev. E 88, 062722.
Marko, J.F., Siggia, E.D., 1995. Stretching DNA. Macromolecules 28, 8759–8770.
Matek, C., Ouldridge, T.E., Doye, J.P.K., Louis, A.A., 2015a. Plectoneme tip bubbles: coupled denaturation and writhing in supercoiled DNA. Sci. Rep. 5, 7655.
Matek, C., Šulc, P., Randisi, F., Doye, J.P.K., Louis, A.A., 2015b. Coarse-grained modelling of supercoiled RNA. Rev. Sci. Instrum. 143, 243122.
Matera, A.G., Terns, R.M., Terns, M.P., 2007. Non-coding RNAs: lessons from the small nuclear and small nucleolar RNAs. Nat. Rev. Mol. Cell Biol. 8, 209–220.
Mathew-Fenn, R.S., Das, R., Harbury, P.A.B., 2008. Remeasuring the double helix. Science 322, 446–449.
McIntosh, D.B., Saleh, O.A., 2011. Salt species-dependent electrostatic effects on ssDNA elasticity. Macromolecules 44, 2328–2333.
Moroz, J.D., Nelson, P., 1997. Torsional directed walks, entropic elasticity, and DNA twist stiffness. Proc. Natl. Acad. Sci. U.S.A. 94, 14418–14422.
Moroz, J.D., Nelson, P., 1998. Entropic elasticity of twist storing polymers. Macromolecules, 1–38.
Mosconi, F., Allemand, J.F., Bensimon, D., Croquette, V., 2009. Measurement of the torque on a single stretched and twisted DNA using magnetic tweezers. Phys. Rev. Lett. 102, 078301.
Mosconi, F., Allemand, J.F., Croquette, V., 2011. Soft magnetic tweezers: a proof of principle. Rev. Sci. Instrum. 82, 034302.
Murphy, M.C., Rasnik, I., Cheng, W., Lohman, T.M., Ha, T., 2004. Probing single-stranded DNA conformational flexibility using fluorescence spectroscopy. Biophys. J. 86, 2530–2537.
Nelson, P.C., 2002. Biological Physics: Energy, Information, Life.
Neuman, K.C., Nagy, A., 2008. Single-molecule force spectroscopy: optical tweezers, magnetic tweezers and atomic force microscopy. Nat. Methods.
Oberstrass, F.C., Fernandes, L.E., Bryant, Z., 2012. Torque measurements reveal sequence-specific cooperative transitions in supercoiled DNA. Proc. Natl. Acad. Sci. U.S.A. 109, 6106–6111.
Oberstrass, F.C., Fernandes, L.E., Lebel, P., Bryant, Z., 2013. Torque spectroscopy of DNA: base-pair stability, boundary effects, backbending, and breathing dynamics. Phys. Rev. Lett. 110, 178103.
Odijk, T., 1977. Polyelectrolytes near the rod limit. J. Polym. Sci.: Polym. Phys. Ed.
Odijk, T., 1995. Stiff chains and filaments under tension. Macromolecules 28, 7016–7018.
Ogawa, T., Yogo, K., Furuike, S., Sutoh, K., Kikuchi, A., Kinosita, K., 2015. Direct observation of DNA overwinding by reverse gyrase. Proc. Natl. Acad. Sci. U.S.A. 112, 7495–7500.
Olsen, K., Bohr, J., 2011. The geometrical origin of the strain-twist coupling in double helices. Rev. Sci. Instrum. 1, 012108–012108–7.
Paik, D.H., Perkins, T.T., 2011. Overstretching DNA at 65 pN does not require peeling from free ends or nicks. J. Am. Chem. Soc. 133, 3219–3221.
Pauling, L., Corey, R.B., 1953. A proposed structure for the nucleic acids. Proc. Natl. Acad. Sci. U.S.A.
Rhodes, D., Klug, A., 1980. Helical periodicity of DNA determined by enzyme digestion. Nature 286, 573–578.
Ribeck, N., Saleh, O.A., 2008. Multiplexed single-molecule measurements with magnetic tweezers. Rev. Sci. Instrum. 79, 094301.
Rief, M., Clausen-Schaumann, H., Gaub, H.E., 1999. Sequence-dependent mechanics of single DNA molecules. Nat. Struct. Biol. 6, 346–349.
Roca, J., 2011. The torsional state of DNA within the chromosome. Chromosoma 120, 323–334.
Rothemund, P.W.K., 2006. Folding DNA to create nanoscale shapes and patterns. Nature 440, 297–302.
Rutkauskas, M., Sinkunas, T., Songailiene, I., Tikhomirova, M.S., Siksnys, V., Seidel, R., 2015. Directional R-Loop formation by the CRISPR-Cas surveillance complex cascade provides efficient off-target site rejection. Cell Rep. 10, 1534–1543.
Saleh, O.A., McIntosh, D.B., Pincus, P., Ribeck, N., 2009. Nonlinear low-force elasticity of single-stranded DNA molecules. Phys. Rev. Lett. 102, 068301.
Salerno, D., Brogioli, D., Cassina, V., Turchi, D., Beretta, G.L., Seruggia, D., Ziano, R., Zunino, F., Mantegazza, F., 2010. Magnetic tweezers measurements of the nanomechanical properties of DNA in the presence of drugs. Nucleic Acids Res. 38, 7089–7099.
Salerno, D., Tempestini, A., Mai, I., Brogioli, D., Ziano, R., Cassina, V., Mantegazza, F., 2012. Single-molecule study of the DNA denaturation phase transition in the force-torsion space. Phys. Rev. Lett. 109, 118303.
Sarkar, A., Leger, J.F., Chatenay, D., Marko, J.F., 2001. Structural transitions in DNA driven by external force and torque. Phys. Rev. E Stat. Nonlin. Soft Matter Phys. 63, 051903.
Schöpflin, R., Brutzer, H., Müller, O., Seidel, R., Wedemann, G., 2012. Probing the elasticity of DNA on short length scales by modeling supercoiling under tension. Biophys. J. 103, 323–330.
Schurr, J.M., 2015. A possible cooperative structural transition of DNA in the 0.25–2.0 pN range. J. Phys. Chem. Lett. 119, 6389–6400.
Schuwirth, B.S., Borovinskaya, M.A., Hau, C.W., Zhang, W., Vila-Sanjurjo, A., Holton, J.M., Cate, J.H.D., 2005. Structures of the bacterial ribosome at 3.5 A resolution. Science 310, 827–834.
Selvin, P.R., Cook, D.N., Pon, N.G., Bauer, W.R., Klein, M.P., Hearst, J.E., 1992. Torsional rigidity of positively and negatively supercoiled DNA. Science 255, 82–85.
Sheinin, M.Y., Wang, M.D., 2009. Twist–stretch coupling and phase transition during DNA supercoiling. J. Phys. Chem. 11, 4800–4803.
Sheinin, M.Y., Forth, S., Marko, J.F., Wang, M.D., 2011. Underwound DNA under tension: structure, elasticity, and sequence-dependent behaviors. Phys. Rev. Lett. 107, 108102.
Sheinin, M.Y., Li, M., Soltani, M., Luger, K., Wang, M.D., 2013. Torque modulates nucleosome stability and facilitates H2A/H2B dimer loss. Nat. Commun. 4, 2579.
Sim, A.Y., Lipfert, J., Herschlag, D., Doniach, S., 2012. Salt dependence of the radius of gyration and flexibility of single-stranded DNA in solution probed by small-angle X-ray scattering. Phys. Rev. E Stat. Nonlin. Soft Matter Phys. 86, 021901.
Sischka, A., Toensing, K., Eckel, R., Wilking, S.D., Sewald, N., Ros, R., Anselmetti, D., 2005. Molecular mechanisms and kinetics between DNA and DNA binding ligands. Biophys. J. 88, 404–411.
Skolnick, J., Fixman, M., 1977. Electrostatic persistence length of a wormlike polyelectrolyte. Macromolecules 10, 944–948.
Smith, S.B., Finzi, L., Bustamante, C., 1992. Direct mechanical measurements of the elasticity of single DNA molecules by using magnetic beads. Science 258, 1122–1126.

Smith, S.B., Cui, Y., Bustamante, C., 1996. Overstretching B-DNA: the elastic response of individual double-stranded and single-stranded DNA molecules. Science 271, 795–799.
Storm, C., Nelson, P.C., 2003. Theory of high-force DNA stretching and overstretching. Phys. Rev. E Stat. Nonlin. Soft Matter Phys. 67, 051906.
Strick, T.R., Allemand, J.F., Bensimon, D., Bensimon, A., Croquette, V., 1996. The elasticity of a single supercoiled DNA molecule. Science 271, 1835–1837.
Strick, T.R., Croquette, V., Bensimon, D., 1998. Homologous pairing in stretched supercoiled DNA. Proc. Natl. Acad. Sci. U.S.A. 95, 10579–10583.
Strick, T., Allemand, J., Croquette, V., Bensimon, D., 2000. Twisting and stretching single DNA molecules. Prog. Biophys. Mol. Biol. 74, 115–140.
Tama, F., Valle, M., Frank, J., Brooks, C.L., 2003. Dynamic reorganization of the functionally active ribosome explored by normal mode analysis and cryo-electron microscopy. Proc. Natl. Acad. Sci. U.S.A. 100, 9319–9323.
Taylor, P., Rixon, F., Desselberger, U., 1985. Rise per base pair in helices of double-stranded rotavirus RNA determined by electron microscopy. Virus Res. 2, 175–182.
Tempestini, A., Cassina, V., Brogioli, D., Ziano, R., Erba, S., Giovannoni, R., Cerrito, M. G., Salerno, D., Mantegazza, F., 2013. Magnetic tweezers measurements of the nanomechanical stability of DNA against denaturation at various conditions of pH and ionic strength. Nucleic Acids Res. 41, 2009–2019.
Thomas, T.J., Bloomfield, V.A., 1983. Chain flexibility and hydrodynamics of the B and Z forms of poly(dG-dC).poly(dG-dC). Nucleic Acids Res. 11, 1919–1930.
van Loenhout, M.T.J., de Grunt, M.V., Dekker, C., 2012a. Dynamics of DNA supercoils. Science 338, 94–97.
van Loenhout, M.T.J., Kerssemakers, J.W.J., De Vlaminck, I., Dekker, C., 2012b. Non-bias-limited tracking of spherical particles, enabling nanometer resolution at low magnification. Biophys. J. 102, 2362–2371.
van Mameren, J., Gross, P., Farge, G., Hooijman, P., Modesti, M., Falkenberg, M., Wuite, G.J.L., Peterman, E.J.G., 2009. Unraveling the structure of DNA during overstretching by using multicolor, single-molecule fluorescence imaging. Proc. Natl. Acad. Sci. U.S.A. 106, 18231–18236.
van Oene, M.M., Dickinson, L.E., Pedaci, F., Köber, M., Dulin, D., Lipfert, J., Dekker, N. H., 2015. Biological magnetometry: torque on superparamagnetic beads in magnetic fields. Phys. Rev. Lett. 114, 218301.
Vladescu, I.D., McCauley, M.J., Nuñez, M.E., Rouzina, I., Williams, M.C., 2007. Quantifying force-dependent and zero-force DNA intercalation by single-molecule stretching. Nat. Methods 4, 517–522.
Vlijm, R., Lee, M., Lipfert, J., Lusser, A., Dekker, C., Dekker, N.H., 2015a. Nucleosome assembly dynamics involve spontaneous fluctuations in the handedness of tetrasomes. Cell Rep. 10, 216–225.
Vlijm, R., Lee, M., Ordu, O., Boltengagen, A., Lusser, A., Dekker, N.H., Dekker, C., 2015b. Comparing the assembly and handedness dynamics of (H3.3-H4)2 tetrasomes to canonical tetrasomes. PLoS ONE 10, e0141267.
Watson, J.D., Crick, F., 1953. Molecular structure of nucleic acids. Nature.
Wenner, J.R., Williams, M.C., Rouzina, I., Bloomfield, V.A., 2002. Salt dependence of the elasticity and overstretching transition of single DNA molecules. Biophys. J. 82, 3160–3169.
Wereszczynski, J., Andricioaei, I., 2006. On structural transitions, thermodynamic equilibrium, and the phase diagram of DNA and RNA duplexes under torque and tension. Proc. Natl. Acad. Sci. U.S.A. 103, 16200–16205.
Williams, M.C., Wenner, J.R., Rouzina, I., Bloomfield, V.A., 2001a. Entropy and heat capacity of DNA melting from temperature dependence of single molecule stretching. Biophys. J. 80, 1932–1939.
Williams, M.C., Wenner, J.R., Rouzina, I., Bloomfield, V.A., 2001b. Effect of pH on the overstretching transition of double-stranded DNA: evidence of force-induced DNA melting. Biophys. J. 80, 874–881.
Wing, R., Drew, H., Takano, T., Broka, C., Tanaka, S., Itakura, K., Dickerson, R.E., 1980. Crystal structure analysis of a complete turn of B-DNA. Nature 287, 755–758.
Winkler, W.C., Breaker, R.R., 2005. Regulation of bacterial gene expression by riboswitches. Annu. Rev. Microbiol. 59, 487–517.
Worcel, A., Strogatz, S., Riley, D., 1981. Structure of chromatin and the linking number of DNA. Proc. Natl. Acad. Sci. U.S.A. 78, 1461–1465.
Yu, Z., Dulin, D., Cnossen, J., Köber, M., van Oene, M.M., Ordu, O., Berghuis, B.A., Hensgens, T., Lipfert, J., Dekker, N.H., 2014. A force calibration standard for magnetic tweezers. Rev. Sci. Instrum. 85, 123114.
Zhang, X., Chen, H., Fu, H., Doyle, P.S., Yan, J., 2012. Two distinct overstretched DNA structures revealed by single-molecule thermodynamics measurements. Proc. Natl. Acad. Sci. U.S.A. 109, 8103–8108.